PIER C

(Received 2 June 2025, Accepted 8 August 2025, Scheduled 20 August 2025)

Imaging Radar Performance: A Comparative Analysis of Multistatic and Monostatic Configurations for Enhanced Detection

Hanane Taourite[1,*], Sidi Mohammed Chouiti[1], and Lotfi Merad[2]

[1] *Laboratory of Telecommunications of Tlemcen (LTT), University of Tlemcen, Algeria*
[2] *Departement de la Formation du Second Cycle, Ecole Supérieure en Sciences Appliquées de Tlemcen, Tlemcen, Algeria*

ABSTRACT: This paper presents a comparative study evaluating the influence of monostatic and multistatic microwave imaging (MWI) configurations on imaging performance. Localization accuracy and Signal-to-Noise Ratio (SNR) are evaluated as key performance metrics for both configurations. Numerical simulations are conducted using CST Studio Suite, considering various scenarios involving circular antenna arrays surrounding embedded metallic rebars of different sizes within concrete pillars of varying geometries. Image reconstruction is performed using Delay-and-Sum Integration (DASI) algorithm, an enhanced version of the conventional Delay-and-Sum (DAS) technique. The simulation results show the performance of the proposed reconstruction technique in terms of localization accuracy.

1. INTRODUCTION

Microwave imaging (MWI) has emerged as a powerful non-invasive technique for subsurface and structural analysis. MWI technology is progressively utilized in biomedical diagnostics [1, 2], agriculture [3], infrastructure [4], mineral sorting [5], and Through-the-Wall imaging [6]. MWI system operates in a contactless manner and utilizes low-power, non-ionizing electromagnetic waves, offering greater operational flexibility and enhanced safety. These advantages, combined with its cost-effectiveness and scalability, position MWI as a promising alternative to conventional ultrasound-based nondestructive testing methods, especially in civil infrastructure applications. The performance of MWI systems can be enhanced through innovations in architectures, processing methodologies, or a combination of both.

In MWI architecture, antenna design is a crucial factor in enhancing performance. The addition of slots in antenna structures, such as lozenges [7] or rectangles [8], optimizes the transmission and reception of electromagnetic waves. Dual-polarization and cross-polarization techniques [9] improve detection orientation and objects discrimination. Additionally, Metamaterial-based designs enhance detection capabilities by incorporating sub-wavelength resonant elements, which effectively reduce mutual coupling between closely spaced antennas and provide a wide impedance bandwidth [10].

In addition to optimizing the MWI architecture, improvements in data collection also depend on the strategic arrangement of antennas. The simplest arrangement is monostatic, where a single antenna is used for both transmitting and receiving signals [11, 12]. Alternatively, multistatic arrangement [13] extends this concept by using multiple transmitting and receiving antennas distributed at different locations. Each configuration has its own advantages and disadvantages, depending on the specific requirements and constraints of the system.

In order to evaluate the imaging performance of each configuration, a few studies have directly compared their imaging performance metrics, but they are limited in number and scope. For instance, the research in [14] offered only a qualitative visual comparison, while simplifying the experimental setup by placing the target above ground. Theoretical analysis in [15] concluded that the two configurations exhibit similar resolution bounds, though multistatic systems yield improved image clarity by reducing side-lobe artifacts. A more detailed comparison in [16] evaluated different multiview and multimonostatic layouts with respect to resolution performance. However, localization accuracy, a crucial metric for precise target identification, remains underexplored in comparative studies.

Furthermore, the majority of existing MWI systems rely on linear antenna arrays, which are well suited for planar or semi-planar scenarios but inherently limited when imaging volumetric structures. Such configurations fail to provide full angular coverage. In this context, we propose the use of circular antenna arrays in both monostatic and multistatic configurations to ensure comprehensive angular sampling. In terms of image reconstruction, we adopt Delay-and-Sum Integration (DASI) algorithm [17], an enhanced version of the traditional Delay-and-Sum (DAS) technique.

Delay-and-Sum Integration (DASI) algorithm has been primarily employed in biomedical applications. In this study, DASI approach is applied to the detection and localization of metallic rebars embedded within concrete structures, an envi-

* Corresponding author: Hanane Taourite (hanane.taourite@univ-tlemcen.dz).

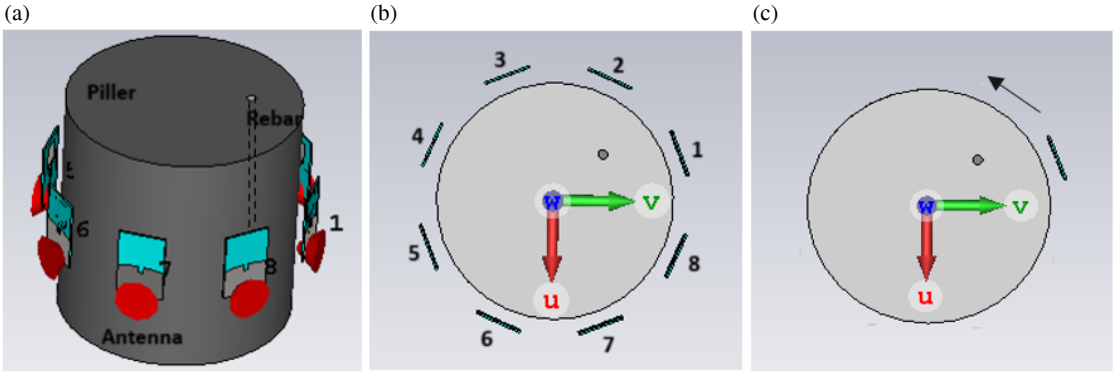

FIGURE 1. Illustration of the simulation model. (a) 3D Representation of the concrete pillar and embedded rebars with antenna positions. (b) Top view of pillar in the multistatic case. (c) Top view of pillar in the monostatic case.

ronment characterized by highly heterogeneous dielectric properties, complex geometries, and pronounced multipath scattering. These conditions differ substantially from those encountered in biological tissues and present challenges for electromagnetic imaging.

A comparative analysis based on one and multiple metallic rebars embedded in a concrete pillar surrounded by antennas will be presented in the cases of monostatic and multistatic configurations to assess localization robustness index across geometries.

The remainder of this paper is structured as follows. Section 2 outlines the DASI reconstruction methodology. Section 3 describes the simulation setup and antenna configurations. Section 4 presents comparative results highlighting the localization performance of both configurations. Section 5 concludes the study and discusses future directions for MWI system development.

2. PROCESSING ALGORITHM

Data processing plays a pivotal role in the performance of MWI approach. In our study, backscattered data were processed using DASI, an enhanced version of DAS algorithm developed by Chouiti et al. [17], selected to assess the impact of each configuration in localization error metric.

Delay-And-Sum Integration (DASI) is a radar-based microwave imaging algorithm that operates on the principle of beamforming. This method involves summing the backscattered signals after applying temporal shifts, then squaring the combined result and integrating it over a designated time interval [17]. If an obscured target is present, its returns add coherently, forming a detectable energy peak, while background clutter is suppressed. Finally, the computed energy values are mapped to generate an image that highlights the presence of obscured target.

This concept can be mathematically formulated as follows [18]:

$$E(r) = \int_0^{T_{win}} \left[\sum_{n=1}^{N} R_n(t - \tau_n(r)) \right]^2 dt \qquad (1)$$

where $E(r)$ Indicates the power at the focal point $r = [x, y]$ within the investigated area. The received signal at the n-th antenna is denoted by $R_n(t)$, and delay $\tau_n(r)$ corresponds to the round-trip travel time between the antenna location r_n and focal point r, calculated as $\tau_n(r) = \frac{2\|r - r_n\|}{v}$. Here, v is the wave propagation speed in the medium, T_{win} the integration window duration, t the integration variable over time, and N the total number of antennas.

3. SIMULATION SETUP

The detailed simulation setup using Computer Simulation Technology (CST) software is shown in Figure 1. The microstrip antenna detailed in [19] is used. In this simulation, the frequency range extends from 3.5 GHz to 5.5 GHz, with an operating frequency of 4.1 GHz. Given the complexity of the scenario, the concrete pillar is modeled as the background medium for all simulation cases. One of the key challenges in this context is the accurate estimation of the pillar's electromagnetic properties. As a result, the selection of an appropriate permittivity value is a critical factor in ensuring accurate simulation results. The dielectric permittivity of concrete typically ranges from 4 to 7, as reported in [20]. For this study, a value of 6.4 is selected to closely approximate realistic conditions. Additionally, metallic rebars embedded within the pillar are considered in the simulation.

The top-view models for both multistatic and monostatic cases are shown in Figure 1. In the multistatic setup, eight antennas are uniformly distributed around the pillar in a circular arrangement, with a spacing of approximately $\lambda/3$ between antennas, where λ corresponds to a frequency of 4.1 GHz. The distance between the pillar and antennas is 5 mm. With a normalized excitation signal, a monopole antenna (Antenna 1) transmits a pulse into the cylindrical pillar. Then, the backscattered signals are received by all receiving antennas, Rx_j, where $j = 1, \ldots, 8$, as shown in Figure 1(b). The monostatic data were acquired at the same locations as in the multistatic configuration, following the scanning direction illustrated in Figure 1(c).

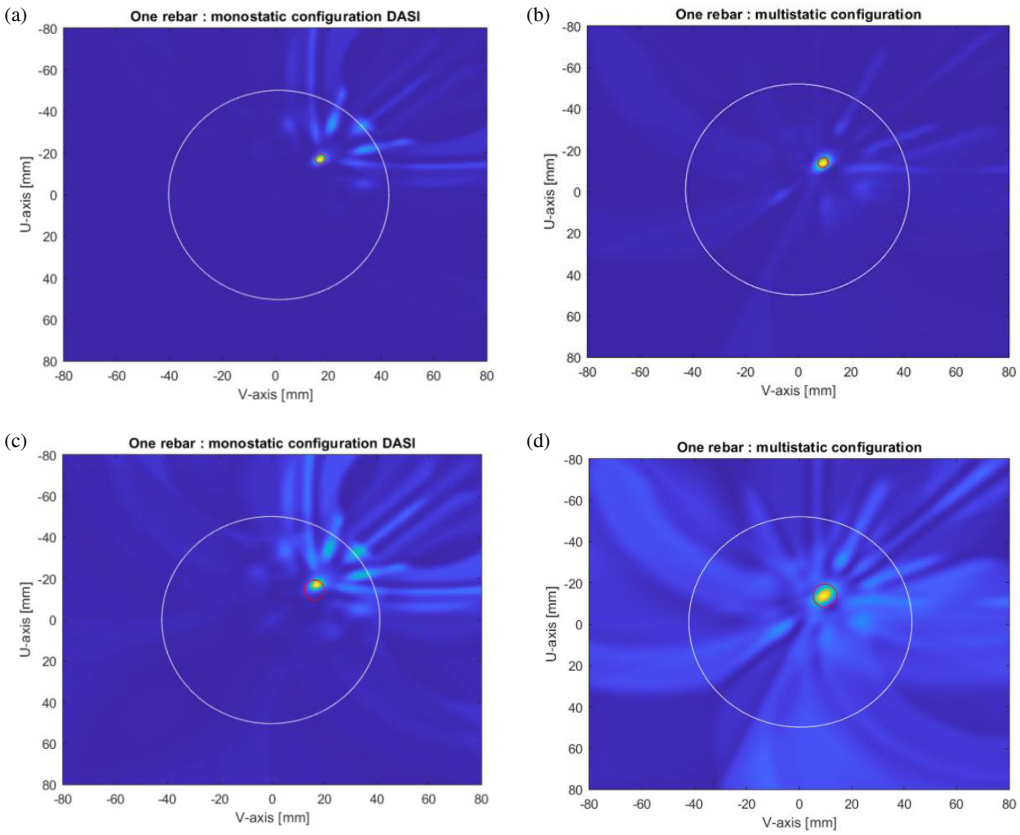

FIGURE 2. Reconstructed images of a single rebar embedded in a concrete pillar. (a) Monostatic configuration, 6 mm rebar. (b) Multistatic configuration, 6 mm rebar. (c) Monostatic configuration, 12 mm rebar. (d) Multistatic configuration, 12 mm rebar. Red circles indicate the true rebar positions.

4. RESULTS AND DISCUSSION

4.1. Evaluation of Localization Accuracy and Signal-to-Noise Ratio (SNR) in Monostatic and Multistatic Configurations

To evaluate the localization accuracy of the embedded metallic rebar, two cases were considered. One with a diameter of 6 mm (Figures 2(a), (b)) and the other with a diameter of 12 mm (Figures 2(c), (d)). These diameters were selected to closely resemble real-world structural conditions. Both configurations share identical simulation parameters, as shown in Figure 1, with a varying position of rebar. The collected data were imported into MATLAB for image processing and reconstructing based on the DASI algorithm under both monostatic (Figures 2(a), (c)) and multistatic (Figures 2(b), (d)) configurations.

We observe that when using a rebar with a diameter of either 6 mm or 12 mm, the reconstructed images exhibit qualitative similarity in the two configurations.

To quantitatively assess the influence of antenna configuration on localization accuracy and signal quality, a 12 mm rebar was placed at multiple known positions. The localization error for both the monostatic and multistatic configurations was calculated using the Euclidean distance between the real position of the target (as defined in the CST simulation) and the detected position in the reconstructed image. The following formula was used:

$$Error = \sqrt{(x_{real} - x_{detected})^2 + (y_{real} - y_{detecte})^2} \quad (2)$$

where:

- (x_{real}, y_{real}) describes the true position of the embedded rebar;
- $(x_{detected}, y_{detected})$ describes the position of the maximum intensity in the reconstructed image, indicating the detected target location.

The localization performance and associated signal-to-noise ratios (SNRs) for the selected target positions are summarized in Table 1. When the target was located at the center of the pillar (0.00, 0.00), the two configurations achieved identical localization accuracy with zero error, indicating equivalent performance under symmetric and ideal conditions. However, as the target was moved away from the center, a slight degradation in localization precision was observed in both configurations, with error values increasing to 2.12 mm at the most offset location (10.00, −10.00). Notably, the multistatic configuration consistently exhibited higher SNR across all test cases, with a maximum of 42.04 dB at the central position, than 33.59 dB for the monostatic setup. This trend persisted at off-center locations, with the multistatic system demonstrating superior SNR. These findings suggest that while both configurations yield comparable localization errors under the tested conditions, the multistatic system offers enhanced signal robustness, particularly in terms of SNR. This advantage can be critical in scenar-

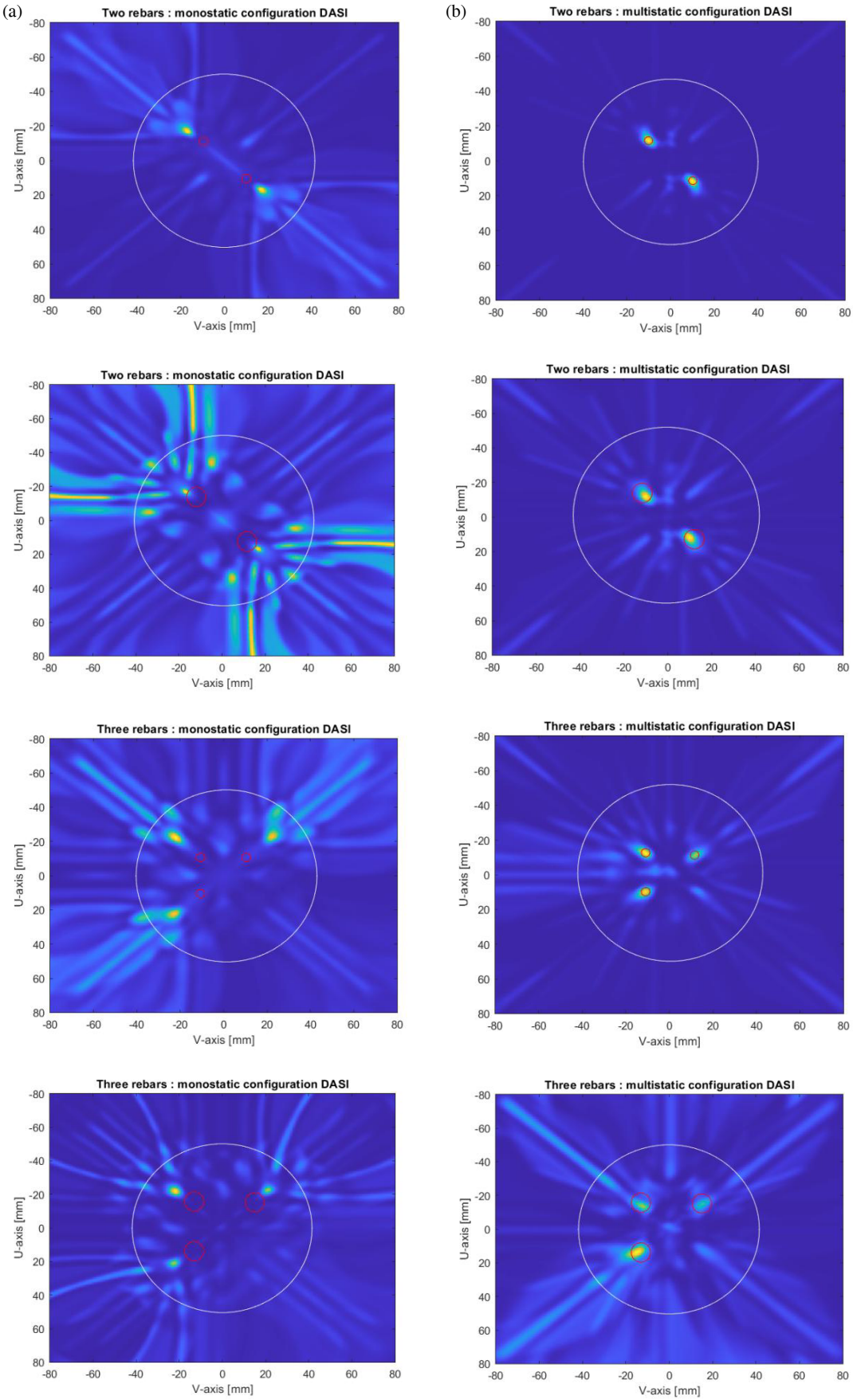

FIGURE 3. Reconstructed images of two and three embedded rebars with diameters of 4 mm and 12 mm. (a) Monostatic setup. (b) Multistatic setup. The red circles illustrate their correct position.

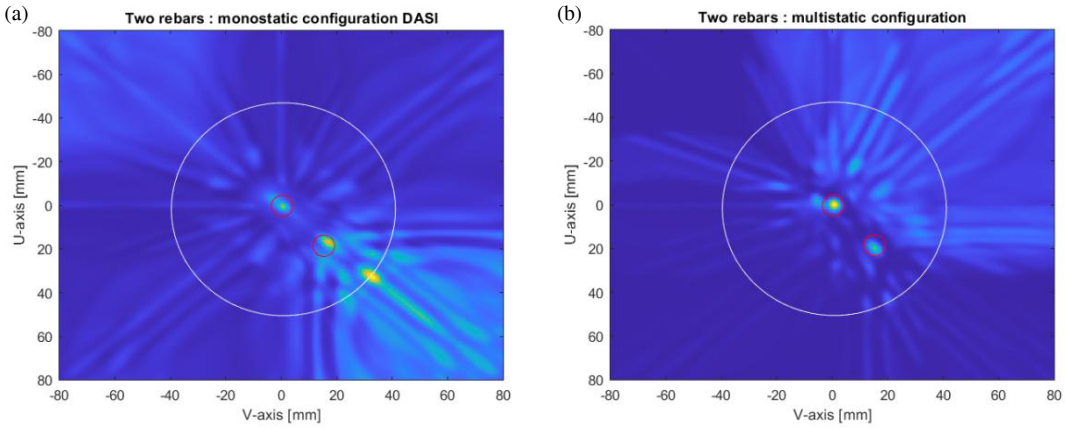

FIGURE 4. Reconstructed images of two embedded rebars with 12 mm diameters, positioned asymmetrically. (a) Monostatic configuration. (b) Multistatic configuration.

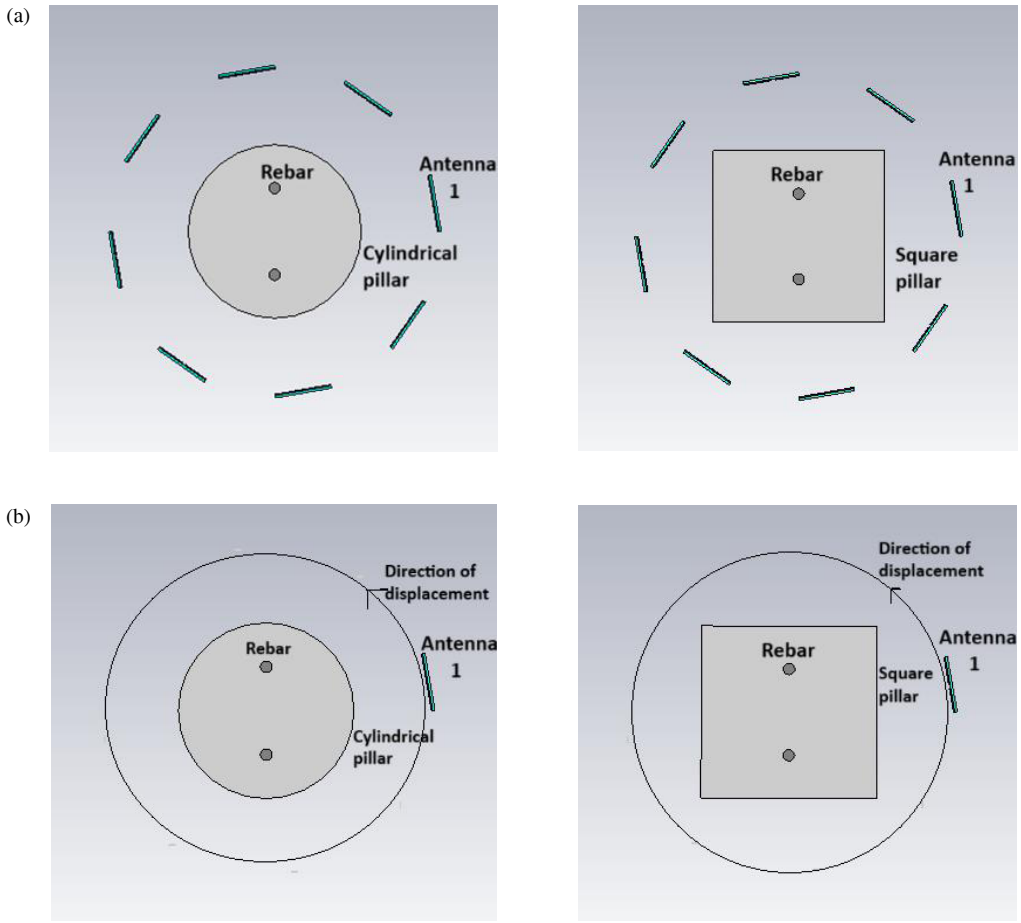

FIGURE 5. Illustration of the top view of the simulation model for square and cylindrical pillars. (a) Multistatic case. (b) Monostatic case.

ios involving complex propagation environments, low-contrast targets, or high noise levels.

To extend this analysis, Figure 3(b) presents reconstructed images for the multistatic configuration in the presence of multiple rebars. The rebars, with diameters of 6 mm and 12 mm, are correctly detected, attributed to the spatial diversity provided by distributed antennas. Similarly, as shown in Figure 3(a), the monostatic configuration is capable of detecting multiple rebars of both diameters. However, positional inaccuracies emerge due to overlapping reflections, which can result in hyperbolic interference, leading to reduced localization accuracy. This issue is particularly pertinent when identifying features such as rebar within complex environments, as noted in [21]. Addi-

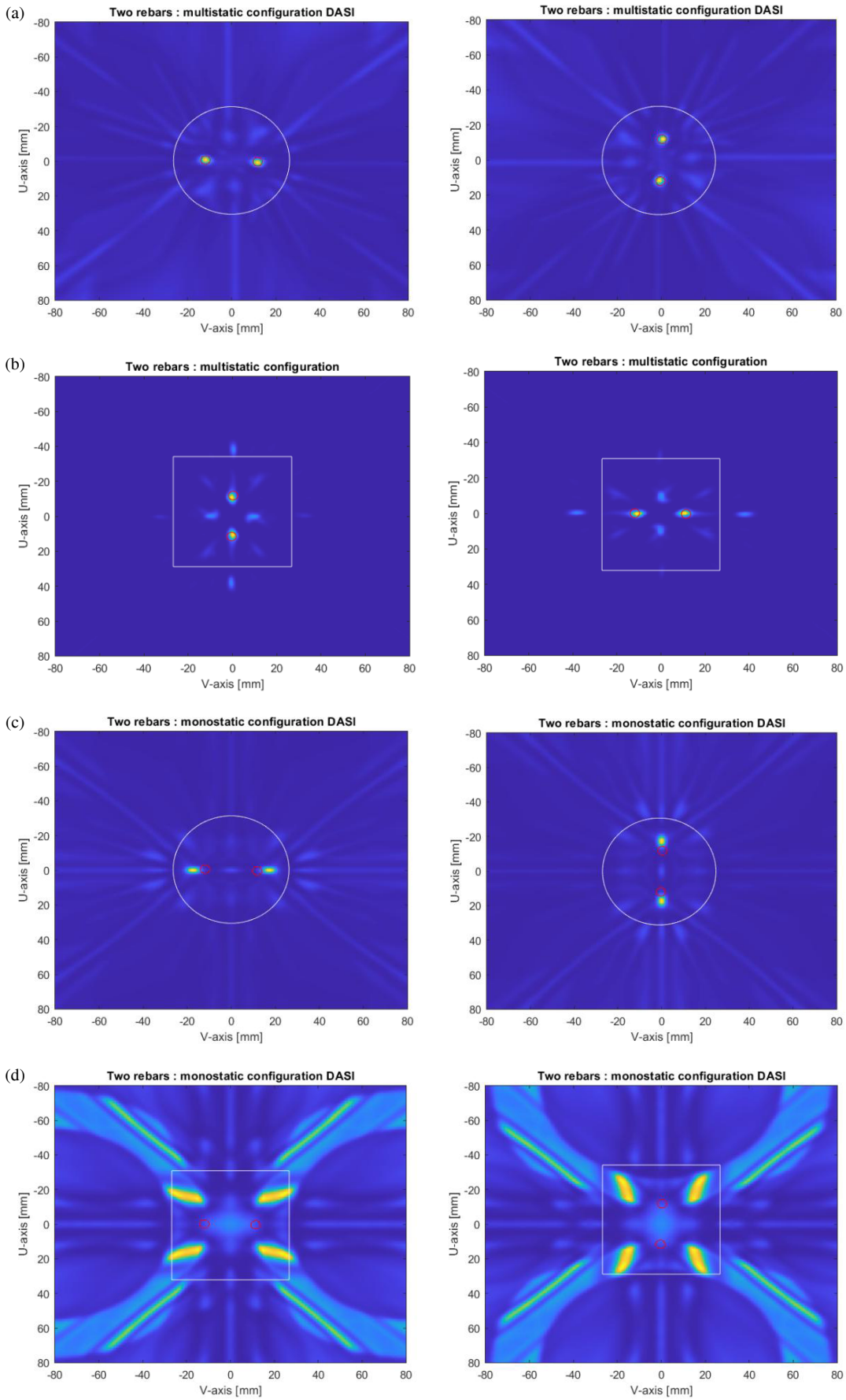

FIGURE 6. Reconstructed images for two embedded rebars. (a) Cylindrical pillar in the multistatic case. (b) Square pillar in the multistatic case. (c) Cylindrical pillar in the monostatic case. (d) Square pillar in the monostatic case.

TABLE 1. Comparison of localization accuracy and signal-to-noise ratio (SNR) for multistatic and monostatic configurations at different target positions.

Real Position (mm)	Detected Position (mm) — Multistatic	Localization Error (mm) — Multistatic	Detected Position (mm) — Monostatic	Localization Error (mm) — Monostatic	SNR (dB) — Multistatic	SNR (dB) — Monostatic
0.00, 0.00	0.00, 0.00	0.00	0.00, 0.00	0.00	42.04	33.59
5.00, −5.00	6.00, −6.00	1.41	6.00, −6.00	1.41	40.41	31.30
10.00, −10.00	11.50, −11.50	2.12	11.50, −11.50	2.12	37.59	25.46

tionally, when the diameter is 12 mm, we observe an increase in artifacts due to raised scattering effects.

To further evaluate the robustness of the proposed multistatic configuration-based DASI algorithm, additional simulations were conducted under asymmetrical conditions, wherein the rebars were positioned irregularly with respect to the center of the pillar. This configuration introduces increased complexity due to the absence of geometric symmetry. As illustrated in Figure 4, the multistatic configuration continues to demonstrate reliable detection and high localization fidelity performance, even under these non-ideal conditions. Although minor shifts in target localization were observed compared to the symmetrical case, the overall image quality remains consistent. In contrast, the monostatic configuration exhibits reduced detection performance and increased artifacts, primarily due to the lack of symmetry, which typically supports constructive interference and improved focusing.

4.2. Influence of Pillar Geometry on Localization Accuracy

In order to show the robustness of each configuration against structural geometry, simulations were performed using the same antenna arrangement described previously in Figure 1. Two rebars with diameters of 6 mm were oriented vertically and horizontally at coordinates $(\pm 15, 0)$ mm and $(0, \pm 15)$ mm, respectively. The cylindrical pillar had a diameter of 60 mm, while the square pillar had a side length of 60 mm as presented in Figure 5.

Figures 6(a) and 6(b) demonstrate that the spatial diversity of the multistatic configuration effectively detects both the number and positions of metallic rebars in cylindrical and square pillars. However, the monostatic configuration, as illustrated in Figures 6(c) and 6(d), can only detect rebars in the cylindrical pillar and fails in the square pillar due to strong reflections and secondary propagation paths caused by its flat surfaces and sharp edges.

These results highlight the importance of antenna configuration in relation to structural geometry. While monostatic systems may suffice in homogeneous or symmetric media, multistatic configurations are better suited to environments with irregular or highly reflective boundaries. The results also show that the geometry of the medium significantly affects localization accuracy, even when the dielectric properties are identical.

5. CONCLUSION

In this study, the impact of the proposed antenna configuration on the imaging accuracy of the MWI approach has been explored. A comparative analysis based on one and multiple metallic rebars embedded in a concrete pillar surrounded by antennas has been presented in the cases of monostatic and multistatic configurations. The simulation results demonstrate that a multistatic circular configuration significantly enhances the localization accuracy of multiple embedded rebars in pillars of different shapes compared to an equivalent monostatic configuration. Conversely, in single target scenarios, the monostatic configuration achieves more accurate localization than its multistatic counterpart, primarily due to its simpler signal paths and reduced susceptibility to calibration errors. In future work, we aim to incorporate metamaterial-based antenna designs to further enhance imaging performance and to conduct experimental validation of the proposed configurations.

REFERENCES

[1] Lalitha, K. and J. Manjula, "Non-invasive microwave head imaging to detect tumors and to estimate their size and location," *Physics in Medicine*, Vol. 13, 100047, Jun. 2022.

[2] Ismail, D. and S. Mustafa, "Diagnosis of a brain stroke using wideband microwave scattering," *Royal Society Open Science*, Vol. 10, No. 3, Mar. 2023.

[3] Garvin, J., F. Abushakra, Z. Choffin, B. Shiver, Y. Gan, L. Kong, and N. Jeong, "Microwave imaging for watermelon maturity determination," *Current Research in Food Science*, Vol. 6, 100412, 2023.

[4] Suzuki, K., S. Nakamura, and S. Kidera, "Complex permittivity retrieval approach with radar enhanced contrast source inversion for microwave nondestructive road evaluation," *IEEE Journal of Selected Topics in Applied Earth Observations and Remote Sensing*, Vol. 17, 476–488, 2024.

[5] Duan, B., E. R. Bobicki, and S. V. Hum, "Application of microwave imaging in sensor-based ore sorting," *Minerals Engineering*, Vol. 202, 108303, Nov. 2023.

[6] Doğu, S., "Investigation of detectabilities of the dielectric objects in a through-the-wall microwave imaging setup," in *2023 31st Signal Processing and Communications Applications Conference (SIU)*, 1–4, Istanbul, Turkiye, Jul. 2023.

[7] Sivasankari, S., P. Raja, and N. Saranya, "A ultra-wideband vivaldi antenna with lozenge shaped slots for biomedical applications," in *2023 International Conference on System, Computation, Automation and Networking (ICSCAN)*, 1–5, Puducherry,

India, 2023.

[8] Hammouch, N., A. Rghioui, H. Ammor, M. Oubrek, and J. Lloret, "A low-cost uwb microwave imaging system for early-stage breast cancer detection," *Multimedia Tools and Applications*, Vol. 84, No. 17, 17 329–17 360, Jul. 2025.

[9] Abou-Khousa, M. A., M. S. U. Rahman, and X. Xingyu, "Dual-polarized microwave imaging probe," *IEEE Sensors Journal*, Vol. 19, No. 5, 1767–1776, Mar. 2019.

[10] Alibakhshikenari, M., B. S. Virdee, P. Shukla, N. O. Parchin, L. Azpilicueta, C. H. See, R. A. Abd-Alhameed, F. Falcone, I. Huynen, T. A. Denidni, and E. Limiti, "Metamaterial-inspired antenna array for application in microwave breast imaging systems for tumor detection," *IEEE Access*, Vol. 8, 174 667–174 678, 2020.

[11] Kwon, S. and S. Lee, "Recent advances in microwave imaging for breast cancer detection," *International Journal of Biomedical Imaging*, Vol. 2016, No. 1, 5054912, 2016.

[12] Fear, E. C., J. Bourqui, C. Curtis, D. Mew, B. Docktor, and C. Romano, "Microwave breast imaging with a monostatic radar-based system: A study of application to patients," *IEEE Transactions on Microwave Theory and Techniques*, Vol. 61, No. 5, 2119–2128, May 2013.

[13] Ambrosanio, M., M. T. Bevacqua, T. Isernia, and V. Pascazio, "Performance analysis of tomographic methods against experimental contactless multistatic ground penetrating radar," *IEEE Journal of Selected Topics in Applied Earth Observations and Remote Sensing*, Vol. 14, 1171–1183, 2021.

[14] Zhuravlev, A., V. Razevig, S. Ivashov, A. Bugaev, and M. Chizh, "Experimental comparison of multi-static and mono-static antenna arrays for subsurface radar imaging," in *2015 IEEE International Conference on Microwaves, Communications, Antennas and Electronic Systems (COMCAS)*, 1–4, Tel Aviv, Israel, Nov. 2015.

[15] Naghibi, A. and A. R. Attari, "Near-field radar-based microwave imaging for breast cancer detection: A study on resolution and image quality," *IEEE Transactions on Antennas and Propagation*, Vol. 69, No. 3, 1670–1680, Mar. 2021.

[16] Masoodi, M., G. Gennarelli, F. Soldovieri, and I. Catapano, "Multiview multistatic vs. multimonostatic three-dimensional ground-penetrating radar imaging: A comparison," *Remote Sensing*, Vol. 16, No. 17, 3163, 2024.

[17] Chouiti, S. M., L. Merad, S. M. Meriah, X. Raimundo, and A. Taleb-Ahmed, "An efficient image reconstruction method for breast cancer detection using an ultra-wideband microwave imaging system," *Electromagnetics*, Vol. 36, No. 4, 225–235, May 2016.

[18] Byrne, D., M. O'Halloran, M. Glavin, and E. Jones, "Data independent radar beamforming algorithms for breast cancer detection," *Progress In Electromagnetics Research*, Vol. 107, 331–348, 2010.

[19] Seladji, N., F. Z. Marouf, L. Merad, S. M. Meriah, F. T. Bendimerad, M. Bousahla, and N. Benahmed, "Antenne microruban miniature ultra large bande ULB pour imagerie micro-onde," *Revue Méditerranéenne des Télécommunications*, Vol. 3, No. 1, 21–25, 2013.

[20] González-López, G., S. Blanch, J. Romeu, and L. Jofre, "Debye frequency-extended waveguide permittivity extraction for high complex permittivity materials: Concrete setting process characterization," *IEEE Transactions on Instrumentation and Measurement*, Vol. 69, No. 8, 5604–5613, Aug. 2020.

[21] Li, C., Y. Zhang, L. Wang, W. Zhang, X. Yang, and X. Yang, "Recognition of rebar in ground-penetrating radar data for the second lining of a tunnel," *Applied Sciences*, Vol. 13, No. 5, 3203, Jan. 2023.